RSC Advances

PAPER

View Article Online
View Journal | View Issue

Cite this: *RSC Adv.*, 2024, **14**, 7655

Innovative snail-mucus-extract (SME)-coated nanoparticles exhibit anti-inflammatory and anti-proliferative effects for potential skin cancer prevention and treatment†

Consoli Valeria,[ab] Petralia Salvatore,[ac] Vanella Luca,[ab] Gulisano Maria,[a] Maugeri Ludovica,[a] Satriano Cristina,[d] Montenegro Lucia,[ab] Castellano Angela[e] and Sorrenti Valeria *[ab]

Nowadays, several studies have highlighted the ability of snail mucus in maintaining healthy skin conditions due to its emollient, regenerative and protective properties. In particular, mucus derived from *H. aspersa muller* has been reported to have beneficial effects such as antioxidant, antimicrobial activity and wound repair capacity. To enhance antioxidant activity of snail mucus, it was extracted in a hydroalcoholic solution and consequently freeze-dried. The obtained snail mucus extract (SME) was indeed endowed with higher antioxidant activity observed in cell-free models, however it was not possible to test its effects in cellular models as it creates a thick film on the cell surface. Therefore, in order to enhance beneficial effects of snail mucus and extend its potential use, SME was used to develop snail mucus extract-coated gold nanoparticles (AuNPs-SME) which exhibited anti-inflammatory properties on non-tumorigenic cells. LPS-induced inflammation in human NCTC keratinocytes was used as model to investigate the *in vitro* cytoprotective effects of nanoparticles. Co-treatment with LPS and AuNPs-SME significantly reduced pro-inflammatory cytokine transcription. Moreover, we demonstrated that AuNPs-SME not only can be used for anti-inflammatory treatments, but also as a sunscreen and antioxidant for potential cosmetic applications. Furthermore, AuNPs-SME's ability to selectively inhibit the growth of two human melanoma cell lines without affecting immortalized human keratinocyte viability in the same conditions was assessed. Thus, we demonstrated that snail mucus is suitable for creating innovative formulations and it can be considered a valid candidate for cosmeceutical applications to enrich the snail mucus based anti-age and sunscreen products already present on the market. Moreover, innovative formulations containing snail mucus can be potentially used for the treatment of specific skin neoplasms.

Received 11th January 2024
Accepted 23rd February 2024

DOI: 10.1039/d4ra00291a

rsc.li/rsc-advances

Introduction

Land helix mucus use in medicine has been described by several studies highlighting the ability of snail mucus in maintaining healthy skin conditions thanks to its emollient, regenerative and protective properties. In particular, mucus derived from *H. aspersa muller* has been reported to have beneficial properties such as antimicrobial activity and wound repair capacity.[1–3] It has been reported that snail mucus is able to repair the signs of photoaging by stimulating the formation of collagen, elastin and dermal components. Moreover, it is able to counteract the damage generated by free radicals thanks to the presence of hyaluronic acid and antioxidants.[4] Helix mucus is rich in bioactive compounds such as allantoin, helicidine and helix pomatia agglutinin. Allantoin, also called 5-ureidohydantoin, is used as active ingredient in cosmetics, thanks to its keratolytic effects, the ability to increase the water content of the extracellular matrix and the capacity to enhance wound healing. Helicidine is a mucoglycoprotein able to induce broncho-relaxant effect which is associated with the release of E2 prostaglandins.[5] Helix pomatia agglutinin (HPA) is a *N*-acetylgalactosamine (GalNAc) used as a prognostic indicator for some types of cancer, such as colon and breast tumors, since HPA-associated glycoproteins are linked to metastasis of cancers.[6–8]

[a]*Department of Drug and Health Sciences, University of Catania, Via Santa Sofia 64, 95125 Catania, Italy. E-mail: sorrenti@unict.it*
[b]*CERNUT-Research Centre for Nutraceuticals and Health Products, University of Catania, 95125 Catania, Italy*
[c]*CNR-Institute of Biomolecular Chemistry, Via Paolo Gaifami 18, 95126 Catania, Italy*
[d]*NanoHybrid Biointerfaces Laboratory (NHBIL), Department of Chemical Sciences, University of Catania, Viale Andrea Doria, 6, 95125 Catania, Italy*
[e]*Mediterranean Nutraceutical Extracts (Medinutrex), Via Vincenzo Giuffrida 202, 95128 Catania, Italy*

† Electronic supplementary information (ESI) available. See DOI: https://doi.org/10.1039/d4ra00291a

However, despite the multiple beneficial effects, poor pharmacokinetics of the main bioactive compounds found in snail mucus limit their therapeutic applications. Thus, nanotechnological formulations can be useful for improving their bioavailability.[9] To date, only few studies have reported the development of nanotechnological formulations containing snail slime.[10–14] Moreover, recent works reported snail slime extracted from *Helix Aspersa* snails employment as bio-reducing agent to obtain silver and biogenic gold nanoparticles by green, fast and economical synthesis.

It has been reported that green synthesized gold nanoparticles can exhibit antimicrobial and antioxidant activities, together with skin-lightening, anti-inflammatory and sunscreen properties,[10,11] while green synthesized silver nanoparticles were proved to be effective in inhibiting bacterial growth as well as cancer cells proliferation.[13,14]

In this context, snail mucus among others, has gained interest for the development of novel naturally derived nanomaterials for different applications, due to improved biocompatibility and biodegradability. In particular, innovative nanomaterials as carbon dots and biopolymers have arisen as interesting alternatives to conventional synthetic materials. Interesting examples have been reported by Das and colleagues who exploited various wastes as sources of biopolymers for the development of UV-resistant polymeric thin films applicable to food and textile industry together with biomedical field.[15,16] Additionally, chitin-enriched biopolymers derived from seafood wastes have recently been reported to be a useful alternative for encapsulation of poorly bioavailable compounds as curcumin. Moreover, Md. Asad Khan *et al.*[17] reported that the encapsulation of curcumin within chitosan nanoparticles improved its bioavailability and suggested that curcumin loaded nanoformulations, might be promising candidates in cancer therapy. Fedaa Adaileh *et al.*[18] demonstrated that curcumin-loaded γ-cyclodextrin-grafted hyaluronic acid nanoassimblies can be a promising nanocarrier for clinically useful hydrophobic molecules.

Thus, exploiting innovative nanotechnologies can be the key for the development of more effective cancer treatments, indeed nanostructures offer the benefit of targeted anticancer therapy together with the possibility of specific accumulation in cancer tissues due to leaky nature of tumor vasculature.[19,20]

Hybrid nanostructures combining the physical and chemical properties of more classes of nanomaterials as metal nanoparticles, graphene-oxide nanosheet, thermos-responsive polymers and calix-macrocycles hold great promise for biomedical application.[21–23]

In this context, equipping gold-nanoparticles (AuNPs) with various nanostructures offer good biocompatibility, effective photothermal conversion upon light absorption due to the localized surface plasmon resonance (LSPR) phenomenon and other typical properties of combined nanostructures.

Aim of the present study was to investigate the potential anti-inflammatory and sunscreen properties of gold nanoparticles in immortalized human keratinocyte NCTC cells. In addition, we evaluated the ability of AuNPs-SME to inhibit the growth of two human melanoma cell lines. The novelty of the present work lies on the use of an innovative snail mucus extract obtained by collecting snail mucus through a cruelty-free system and processing it to achieve an extract with higher concentrations of polyphenols compared to snail mucus as it stands, for the development of innovative systems for cancer prevention and treatment.

Results and discussion

Antioxidant activity of snail mucus extract (SME) in cell-free models

Helix mucus is rich in bioactive compounds, however its composition depends on different factors, such as the snail species, feeding and behaviour of the animals. It has been reported that snail mucus is able to counteract the damage generated by free radicals thanks to the presence of hyaluronic acid and antioxidants (Conte *et al.*). As previously reported,[24] low levels of polyphenols justified the poor antioxidant activity of SEM provided by "La lumaca Madonita". To enhance antioxidant activity of snail mucus, it was extracted in a hydroalcoholic solution and subsequently freeze-dried. The extraction method process has allowed to obtain a much higher polyphenol content compared to snail slime. The total phenolic content (TPC) was evaluated spectrophotometrically. The powdered Snail Mucus Extract (SME) was standardized to contain ≥0.3% TPC. SME showed significant antioxidant activity in a concentration-dependent manner, with respect to the scavenger activity of DPPH and inhibition of superoxide anion, as shown in Fig. 6. However, although this extract was endowed with high antioxidant activity in cell-free models, it was not possible to test its effects in cellular models as it created an insoluble film on cell surface. These data are in agreement with Conte *et al.*[9] who reports that the poor pharmacokinetics of the main bioactive compounds of snail mucus, limit their therapeutic applications. Nanotechnological formulations can be useful in improving their bioavailability. Therefore, in order to enhance beneficial effects of snail mucus its extract was then used to develop snail mucus-coated gold nanoparticles (AuNPs-SME).

Gold-nanoparticles-snail-mucus-extract (AuNPs-SME) preparation

In order to obtain nanostructured AuNPs-SME the chemical synthesis was carried out by direct reaction of gold precursor ($HAuCl_4$) with an aqueous dispersion of SME. The known reducing properties of SME induces the reduction process from Au^{III} to Au^0 to form SME capped AuNPs nanostructures. The good stability and the water dispersion of the as prepared gold nanostructures were guaranteed by the SME residue at gold surface. In details, an amount of 150 mg of dried snail-mucus-extract was dispersed in a volume of 100 mL of MilliQ water. Under continuously stirring an aliquot of 750 μL of $HAuCl_4$ 5×10^{-2} M was added and the mixture heated at 70 °C for 90 minutes. The formation of Au-nanostructures was indicated by the reddish-purple colour mixture. The dispersion was separated by centrifugation (13.000 rpm 5 min) and the reddish-purple pellet was washed three times with 1 mL of MilliQ water. Then, the AuNPs-SME was purified by dialysis using

MilliQ water through a dialysis membrane (10 kDa cut off) for 12 hours. Finally, the AuNPs-SME was lyophilized and stored at room temperature. UV-vis optical absorption spectra of AuNPs-SME exhibited the typical LSPR absorption bands for Au-nanostructures at 548 nm and the absorption band at around 272 nm to indicate the presence of snail mucus as capping agent (Fig. 1).

Morphology of AuNPs-SME was investigated by Atomic Force Microscopy investigation (AFM). AFM was used to visualize individual nanoparticles and groups of nanoparticles, indeed, unlike other techniques, it can offer visualization in three dimensions. AFM images for AuNPs-SME sample showed the presence of sphere-like nanostructures (Fig. 2A), the section analysis report a nanostructure size ranging from 5 to 30 nm (Fig. 2C red line). At contrary, AFM images for untreated snail mucus sample showed the presence of sporadic large aggregates with size ranging from 20 to 30 nm (Fig. 2B and C blue line).

The AFM data are in line with the hydrodynamic size obtained by DLS investigations. Indeed, DLS measurements in water evidenced for AuNPs-SME the presence of small nanostructures with hydrodynamic diameter of 6.7 ± 1.5 nm and larger nanostructures sized 100.5 ± 10.1 nm, and a *Z*-potential value of −21.1 ± 2.9 mV. The AuNPs-SME formation was confirmed by FTIR investigation, the Fig. S1† illustrates the FTIR-ATR absorption spectra for SME and for AuNPs-SME samples. In particular, the FTIR signal at about 1613.9 cm^{-1} and in the region 1015–858.2 cm^{-1} and 1555–1530 cm^{-1} observed for the AuNPs-SME sample are diagnostic of the presence of the SME in the Au nanostructures. The AuNPs-SME process formation is mainly based on the reduction properties of the snail mucus, as widely reported for similar natural source in literature.[25] In presence of the snail mucus the Au^{3+} species was rapidly reduced to Au^0 nanostructures as suggested by the UV-vis optical absorption measurements recorded at various reaction times (0, 10 min, 20 min, 30 min 40 min, 50 min, 60 min, 70 min, 80 min and 90 min) whereas the appearance of the typical LSPR band at around 548 nm confirm the Au-nanostructures formation (Fig. 3A). At contrary, the optical absorption spectra recorded for the blank reaction (same experimental conditions but without the snail mucus) did not show the LSPR band, to indicate that the Au-nanostructures formation does not occur in absence of snail mucus (Fig. 3B).

The reductant properties of snail mucus were confirmed by cyclic voltammetry (CV) investigations. The cyclic voltammograms in KCl 0.1 M at pH 7.0 showed the presence of the reduction peak at Ea = − 0.19 V and oxidation peak, at Ec = + 0.18 V (Fig. 4). The reduction potential value of −0.19 V

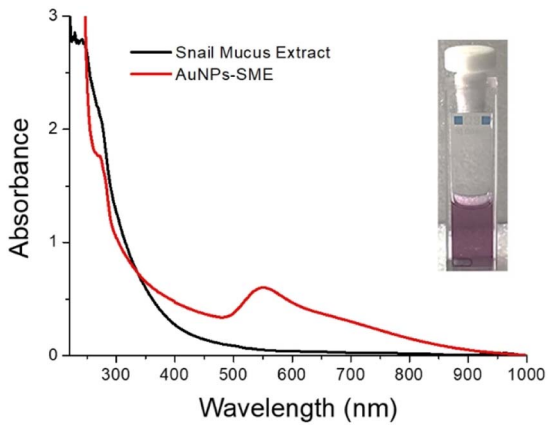

Fig. 1 Optical absorption spectrum of AuNPs-SME and snail-mucus in water. Insets the water dispersion of AuNPs-SME.

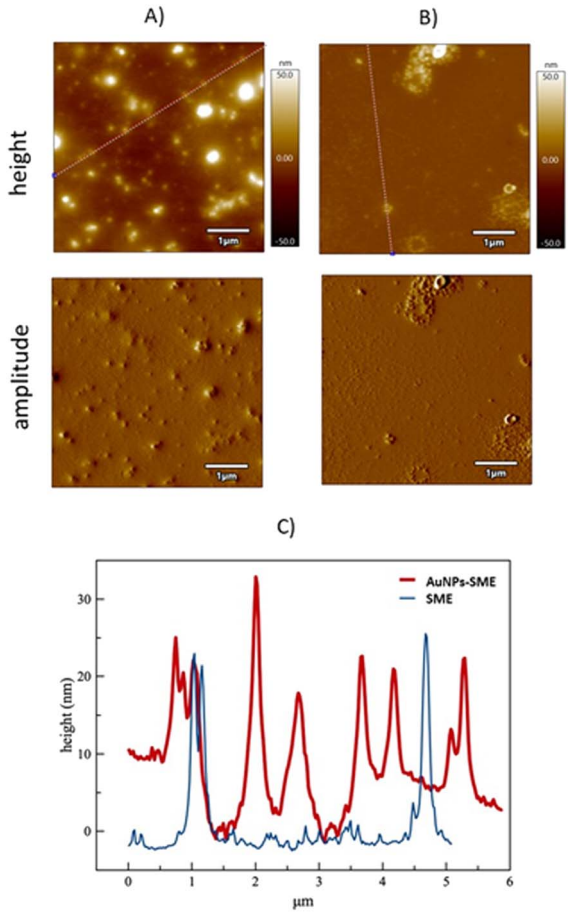

Fig. 2 AFM images: height and amplitude images (5 µm × 5 µm scan size) of AuNPs-SME (A) and SME (B) samples. In (C) the comparison of the section analysis (dashed lines in the height micrographs) for the two samples.

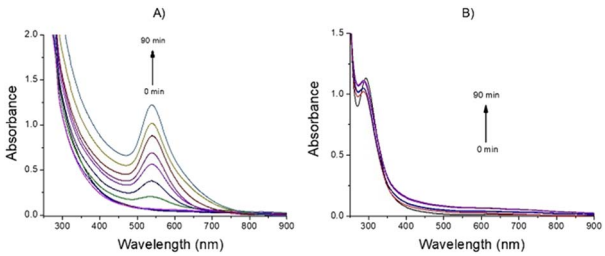

Fig. 3 Optical absorption changes at various reaction times (0, 10 min, 20 min, 30 min 40 min, 50 min, 60 min, 70 min, 80 min and 90 min) and at 70 °C for the AuNPs-SME process formation (A) and for the blank-reaction without SME (B).

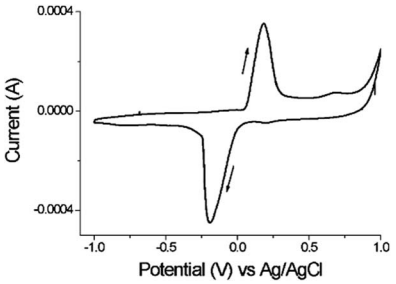

Fig. 4 Cyclic voltammograms for Snail mucus in KCl 0.1 M at pH 7.0 and scan rate 1 V s^{-1}.

observed (closer to the value of standard reductant used for AuNPs formation sodium citrate −0.18 V) is enough to induce the reduction process from Au^{3+} to Au^{0}.

AuNPs-SME photothermal properties

Metallic nanomaterials, as gold, have gained great scientific and technological interest for their key ability to interact with light in the visible to NIR region. When interacting with light at the appropriate wavelengths, free electrons on the metallic nanoparticle surface are excited and conduction-band electrons collectively oscillate at the same frequency. This phenomenon is identified as localized surface plasmon resonance (LSPR). Indeed, gold exhibits photothermal effects arising from their LSPR. To investigate the photothermal properties of AuNPs-SME, an aqueous dispersion (200 μL, Abs_{532nm} = 0.31) was continuously exposed to a 532 nm laser light source. The temperature changes were monitored by a thermal camera. When the temperature of the system reached the maximum, the laser was switched off and the temperature changes during cooling was recorded to confirm the heat transfer of the system. The laser power was measured by a power meter model H410D (Scien-Tech). A photothermal conversion efficiency (η) value of 40.2% with a time constant of 75 s were calculated. To better investigate the correlation between the photothermal activity and the AuNPs-SME amount, experiments using AuNPs-SME dispersions with different absorbance value were performed. The results reported in Fig. 5A indicated temperature increases of about 11.1 °C, 4.6 °C and 2.5 °C for Absorbance (532 nm) values of 0.31, 0.15 and 0.03, respectively. A volume of 200 μL of sample was irradiated with a CW laser 532 nm (power 330 mW) for 5 minutes (Fig. 5A). The power-dependent behaviour was confirmed by the experiments performed with different laser power of 100 mW, 200 mW, and 330 mW, the temperature values increase was about 4.2 °C, 7.6 °C, 8 °C, and 12 °C, respectively (Fig. 5B). Fig. 5C report the time constant calculation. Fig. 5D report the representative thermos-photographs of AuNPs-SME dispersion in water during the photothermal experiments.

Comparison of SME and AuNPs-SME antioxidant activity in cell-free models

In order to evaluate the potential higher antioxidant activity of SME and Au-NPs-SME (due to higher polyphenols content)

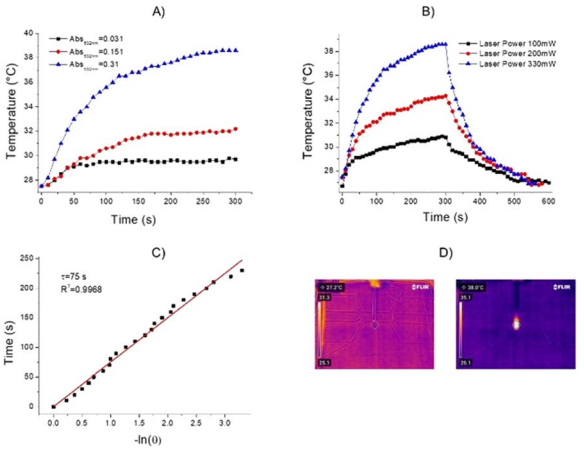

Fig. 5 AuNPs-SME photothermal experiments: (A) photothermal experiments for AuNPs-SME water dispersion at different absorbance values (laser power 330 mW, volume 200 μ); (B) photothermal cycles for AuNPs-SME water dispersion (Abs_{532nm} = 0.31) at different laser power 100 mW, 200 mW and 330 mW; (C) time constant calculation (τ = 75 s) and (D) representative thermophotographs of AuNPs-SME dispersion in water during the photothermal experiments.

compared to snail mucus (previously reported) we performed different cell-free assays. Due to the nature of the bio-organic layer on NPs given by snail mucus extract surrounding Au-core, DPPH stabilization and antioxidant activities were observed. Indeed, the presence of amino acids, proteins and different peptides may be able to exert scavenging activity. In particular, SME abundance in polyphenols and the high content of allantoin and glycolic acid, which have already been reported as strong antioxidants,[26,27] are able to confer scavenging activity to AuNPs-SME (Fig. 7). SME showed significant antioxidant activity in a concentration-dependent manner, with respect to the inhibition of superoxide anion formation, as shown in Fig. 6A, however AuNPs-SME showed a slight SOD-like activity compared to SME (Fig. 6B). In addition, antioxidant activity of SME or gold nanoparticles coated with SME was

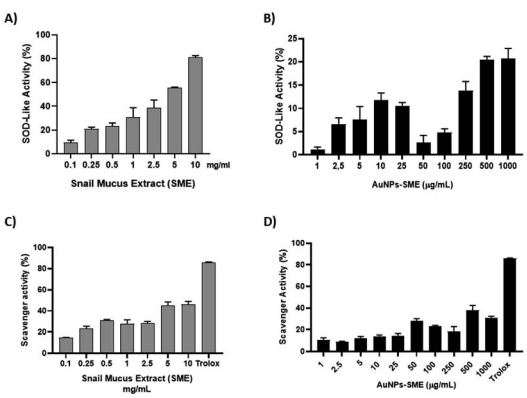

Fig. 6 Evaluation of SME and AuNPs-SME ability of inhibiting superoxide anion formation (A and B) and radical scavenging activity (C and D) in cell-free assays. (Trolox 100 μM was used as positive control for scavenger activity) Results are expressed as mean ± SEM.

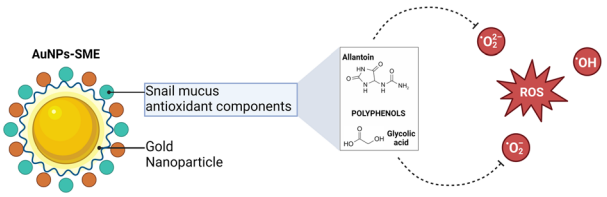

Fig. 7 Schematic representation of AuNPs-SME antioxidant effect.

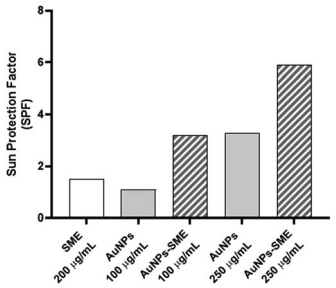

Fig. 8 Sun protection factor (SPF) of snail-mucus-extract (SME), uncoated gold nanoparticles (AuNPs) at different concentrations (100 and 250 μg mL^{-1}) and SME coated AuNPs at different concentrations (100 and 250 μg mL^{-1}).

evaluated also using the DPPH test. The stable free radical DPPH$^{\cdot}$ produced is purple, absorbing at 517 nm. The solution colour changes from purple to yellow when DPPH is all in reduced form, with consequent bleaching of the absorption band of DPPH$^{\cdot}$ at 517 nm. In this case, the reaction was slower than the SOD-Like activity, however, the obtained results occurred dose-response dependent and confirmed the antioxidant activity of the SME (Fig. 6C). AuNPs-SME maintained a similar activity for concentrations down to 50 μg mL^{-1}, which is a very low concentration and therefore their antioxidant capacity is noteworthy (Fig. 6D). This may be due to the high antioxidants concentration of SME which is exploited to synthesize nanoparticles and stabilize them.

Sun protection factor (SPF) of AuNPs-SME

It has been reported that a sunscreen product is able to protect human skin against UV-induced damages thanks to the presence of UV filters as active ingredients. In addition, the use of antioxidants ingredients as additional protection for visible and infrared radiation has also been proposed. As reported by Xian *et al.* the UV-induced skin photodamage is associated with increased ROS (Reactive Oxygen Species) formation and the inactivation of NF-E2-related factor 2 (Nrf2) with consequent impairing the antioxidant defence system inducing cutaneous disorders.[28] Thus, there is growing interest in combining UV-filters properties of antioxidant organic and inorganic compounds to develop hybrid systems as more effective sunscreen formulations.[29,30] As SME coating resulted in AuNPs-SME with high absorption values at wavelength <400 nm, the ability of AuNPs-SME to act as UV filter was explored. The calculation of the sun protection factor (SPF) is commonly used to evaluate the efficacy of sunscreen formulations.[11] As *in vivo* standard methods to determine SPF values in humans are quite expensive and time-consuming, alternative *in vitro* tests that allow obtaining reliable results have been developed.[31–34] In this work, we used the spectrophotometric method based on Mansur equation to determine *in vitro* SPF values as this type of test has already been used to evaluate the photo-protective effects of active ingredients incorporated into nanoparticles.[35] The results of SPF determination are illustrated in Fig. 8. SME at the concentration used in *in vitro* SPF test (200 μg mL^{-1}) did not provide a significant photo-protective activity (SPF = 1.5). Similarly, uncoated AuNPs at different concentrations, 100 and 250 μg mL^{-1}, showed low SPF values (1.1 and 3.3, respectively). However, it is interesting to note that increasing AuNPs concentration raised the SPF value, thus suggesting that the metallic core of AuNPs may act as inorganic sunscreen. The ability of NPs to behave as UV-blockers has already been reported by others studying the effects of lipid nanoparticles as photo-protective agents.[36,37] Coating AuNPs with SME provided a notable increase of SPF value compared with uncoated AuNPs at the same concentration. In particular, about a three-folds increase was observed for AuNPs at 100 μg mL^{-1} (SPF = 3.2) while about a two-folds increase was obtained for AuNPs at 250 μg mL^{-1} (SPF = 5.9). These data suggest a synergic effect between SME coating and NP metallic core that could be useful to design topical formulations with reduced content of synthetic sunscreen agents whose safety for both humans and environment is under debate.

Biological evaluation in cellular models

In order to evaluate potential cytotoxicity of AuNPs-SME, NCTC 2544 cells were treated with different concentrations of gold nanoparticles coated with SME (0.1, 0.5, 1, 2.5, 5, 10, 25, 50, 100, 250 μg mL^{-1} AuNPs-SME) for 48 h and subsequently MTT assay was performed (Fig. 9).

No significant cytotoxic effect was observed. To further assess the possible effects of the AuNPs-SME on the biological inflammatory response, keratinocytes were challenged with LPS and the day after treated with 10 μg mL^{-1} AuNPs-SME. Results showed AuNPs-SME capacity to reduce IL-6 and IL-8 pro-inflammatory cytokines transcription (Fig. 10A and B) and increase anti-inflammatory IL-10 even at low concentrations (10 μg mL^{-1}) (Fig. 10C).

These results suggest that AuNPs-SME may have modulatory effects that could be beneficial in reducing inflammatory or

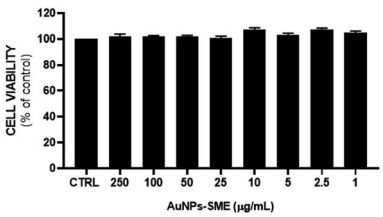

Fig. 9 AuNPs-SME effect on keratinocytes viability after 48 h treatment. Results are expressed as mean ± SEM.

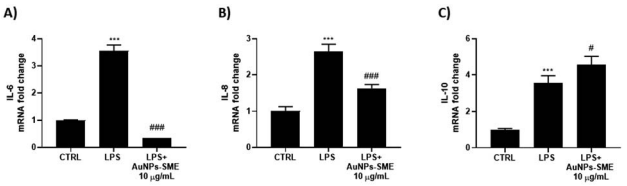

Fig. 10 Evaluation of AuNPs-SME protective effect on a LPS-induced inflammatory model through mRNA levels quantification of interleukins as IL-6 (A), IL-8 (B) and IL-10 (C). Results are expressed as mean ± SEM. (***p < 0.0005 *vs.* CTRL; $^{\#}p$ < 0.05, $^{\#\#\#}p$ < 0.0005 *vs.* LPS-treated group).

pathogenic responses. Moreover, we investigated the possible therapeutic effect of AuNPs-SME against skin cancer. Indeed, ability of AuNPs-SME to inhibit the growth of two human melanoma cell lines, SK-MEL-2 and SK-MEL-5 cells, was evaluated. MTT assay was performed with different concentrations of AuNPs-SME in order to assess its effect on cell viability. Our results showed that after 48 h treatment, AuNPs-SME was not cytotoxic for NCTC 2544 cells non tumorigenic cells whereas it decreased the SK-MEL-2 and SK-MEL-5 human melanoma cell lines viability in a concentration-dependent manner (Fig. 11A and B). A potential explanation may lie behind melanogenesis process involved in tumorigenesis. Indeed, tyrosinase, which is found to be overexpressed in melanoma cells, represents a vital and rate-limiting copper-containing enzyme for melanin biosynthesis.[38,39] Thus, tyrosinase has gained interest as a specific *in situ* weapon which can be potentially used to improve therapeutic efficacy and specificity of melanoma treatment. In this context, it is known that both snail mucus and Au-NPs can affect tyrosinase activity and subsequently act as anticancer agents, indeed it is reasonable to correlate their inhibitory activity towards tyrosinases and selectivity towards melanoma cells instead of keratinocytes, which on the other hand show lower tyrosinase levels and activity.[11,40,41] The highest

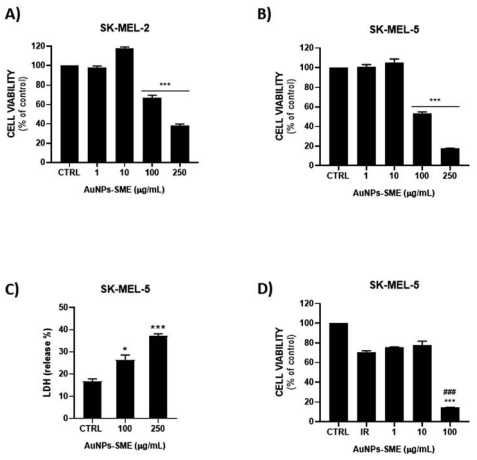

Fig. 11 AuNPs-SME effect on human melanoma cells viability (A and B), measurement of LDH release after treatment with AuNPs-SME highest concentrations (C) and evaluation of NPs potential for PTT (D). Results are expressed as mean ± SEM. (*p < 0.05, ***p < 0.0005 *vs.* CTRL; $^{\#\#\#}p$ < 0.0005 *vs.* IR group: laser irradiated cells).

antiproliferative effect of AuNPs-SME was reached at the concentration of 250 μg mL^{-1}. This effect was more evident for SK-MEL-5 (38% residual vitality) compared to SK-MEL-2 cells (18% residual vitality) (EC50 values reported in Table S1†). Moreover, the standard chemotherapeutic agent 5-FU was tested on both NCTC 2544 and SK-MEL-5 cell lines to verify its cytotoxic effect and compare it to AuNPs-SME. As reported in Fig. S2,† 5-FU treatment resulted in a reduction in both cell lines viability and unlike AuNPs-SME 5-FU did not spare keratinocytes. To investigate molecular mechanisms involved in reduction of SK-MEL-5 cell proliferation, we evaluated the percentage of LDH released into the culture medium as marker of necrosis which results in a disruption of cytoplasmic membrane with the consequent release of cytoplasmic LDH into the medium. As reported in Fig. 11C the presence of 100 and 250 μg mL^{-1} of AuNPs-SME caused a significant increase of LDH release in SK-MEL-5 cells. The highest AuNPs-SME concentration (250 μg mL^{-1}) induced necrosis with about 40% LDH release in the medium. In addition, caspase and apoptosis activation were investigated by using pan-caspase inhibitor (ZVAD-FMK) in combination with AuNPs-SME to assess cell viability, however no significant caspase involvement was observed (data not shown).

Moreover, in order to validate the possible application for photothermal therapy (PTT) in more sensitive human melanoma line (SK-MEL-5), cells were exposed to irradiation treatment alone and in combination with AuNPs-SME at different concentrations (Fig. 11D). Results showed a synergistic effect of AuNPs-SME and photothermia as the combination treatment was able to drastically reduce melanoma cell viability, suggesting AuNPs-SME as potential candidate for PTT in some specific skin cancers.

Materials and methods

General

All chemicals and reagents were used as purchased, without further purification. The cell lines utilized in this study were obtained from Interlab Cell Line Collection Genoa and the American Type Culture Collection (ATCC).

Snail mucus extract (SME). The powdered Snail Mucus Extract (SME) (batch no. 1/22) employed in this study was produced by Medinutrex (Catania, Italy). The Helix aspersa snails were fostered in the private snail farm "La lumaca Madonita" (Campofelice di Roccella 90010—Palermo, Italy, https://www.lumacamadonita.it/, accessed on 10 January 2024). Snail mucus extraction was performed according to a cruelty-free system using the patented extractor machine EXTRACTA as reported in our previous study.[24] Snail Mucus Extract was prepared from Snail Mucus mixed with 60% hydroalcoholic solution (food grade) and then filtered. The filtrate was concentrated at low temperature to remove the solvent and then spray-dried to obtain the standardized extract.

AuNPs-SME synthesis and characterization. All reagents were purchased by Sigma-Aldrich and used as received. Optical absorption UV-Vis-NIR spectra were acquired by spectrophotometer PerkinElmer 365, a quartz cuvette with optical length of

10 mm was used. The particle size and surface charge were examined by using a combined dynamic light scattering and zeta-potential apparatus (DLS, Zetasizer Marvell). The ATR-FTIR spectra for SME and AuNPs-SME were recorded by a FTIR spectrometer equipped with ATR module, model Spectrum two (Perkin Elemer). Atomic Force Microscopy (AFM) imaging was performed in AC mode in air on a commercial AFM instrument (Cypher, Oxford Instruments, Santa Barbara, CA) equipped with a scanner at a *XY* scan range of 30/40 μm (closed/open loop). Silicon cantilevers (OMCL-AC240TS, ~70 kHz, 2 N m^{-1} by Olympus, Japan) were used to acquire scan images in random areas of the samples. To prepare the samples, 10 μL of water dispersion of AuNPs-SME and SME (2.5 mg mL^{-1}) were dispensed on freshly cleaved muscovite mica (Ted Pella, Inc., Redding, CA, USA) and left to dry at room temperature in controlled laboratory environment. AFM images of height were analyzed using the free tool in the MFP-3DTM offline analysis software. Photothermal conversion efficiency (η) was calculated according to equation introduced by Roper *et al.*[42] eqn (1).

$$\eta = \frac{hA\ (T_{max} - T_{surr}) - Q_{Dis}}{I(1 - 10^{-A})} \quad (1)$$

***In vitro* sun protection factor (SPF).** *In vitro* sun protection factor (SPF) values were calculated spectrophotometrically using Mansur equation.[43] Each sample was properly diluted in phosphate buffer pH 7.0 and absorption data were acquired every 5 nm in the range 290–320 nm (spectrophotometer Hitachi U-29009). SPF values were calculated according to the following eqn (2):

$$SPF_{spectrophotometric} = CF \times \sum_{290}^{320} EE(\lambda) \times I(\lambda) \times Abs(\lambda) \quad (2)$$

where CF is the correction factor (=10), EE(λ) is the erythemal effect of the radiation with wavelength λ, $I(\lambda)$ is the solar intensity of radiation with wavelength λ, and Abs(λ) is the absorbance of the sunscreen product at wavelength λ. The values of EE(λ) × $I(\lambda)$ at each wavelength in the range 290–320 nm, determined by Sayre *et al.*,[44] were used to calculated SPF.

DPPH assay. The free radical scavenging activity of the Snail Mucus Extract (SME) and AuNPs-SME was evaluated using the DPPH (2,2-75 diphenyl-1-picrylhydrazyl) assay. The reaction mixtures contained 86 μM DPPH, solubilized in ethanol, and different concentrations of SME (0.1, 0.25, 0.5, 1, 2.5, 5, 10 mg mL^{-1}) and AuNPs-SME (1, 2.5, 5, 10, 25, 50, 100, 250, 500–1000 μg mL^{-1}). After 10 min at room temperature the absorbance at λ = 517 nm was recorded.

SOD-like activity. SOD-like activity was measured using pyrogallol autoxidation method. Briefly, pH 8.2, 50 mM Tris–Cl buffer with 1 mM EDTA was used as a reaction solution. Samples were added to 0.2 mM pyrogallol (dissolved in pH 6.5, 50 mM PPB) to initiate the reaction, and the absorbance decrease of pyrogallol was monitored at 420 nm. The percentage inhibition of pyrogallol autoxidation was calculated as follows:

$$\%\ \text{inhibition of pyrogallol autoxidation} = [1 - (\Delta A/\Delta A_{max})] \times 100$$

where ΔA = absorbance change due to pyrogallol autoxidation in the sample reaction system; ΔA_{max} = absorbance change due to pyrogallol autoxidation in the control (without samples); one unit of SOD activity was defined as the amount required for inhibiting pyrogallol autoxidation by 50% per min.

Cell cultures and treatments. Experiments were conducted on human keratinocyte cell line NCTC 2544 (Interlab Cell Line Collection Genoa, Italy) and human melanoma cell lines SK-MEL-2 and SK-MEL-5 (HTB-68, HBT-70 ATCC, Rockville, MD, USA). Cells were cultured in Eagle's Minimum Essential Medium (EMEM) supplemented with 10% FBS and 1% penicillin–streptomycin and maintained at 37 °C and 5% CO_2. NCTC 2544, SK-MEL-2 and SK-MEL-5 cells were treated with different concentrations of AuNPs-SME for 48 h. In order to evaluate AuNPs-SME anti-inflammatory activity, keratinocytes were also challenged with LPS for 24 h. Subsequently, only melanoma cells were challenged with AuNPs-SME and laser radiation at λ = 808 nm for 5 minutes. NCTC 2544 and SK-MEL-5 cells were also treated with standard chemotherapeutic agent 5-FU at different concentrations (10, 50, 100 μM) for 48 h.

Cell viability assay. To evaluate cell viability cells were seeded into 96-well plates at a density of 7.0 × 103 cells per well in 100 μL of culture medium. After 48 h of treatment, 100 μL of 0.25 mg mL^{-1} 3-(4,5-dimethylthiazol-2-yl)-2, 5-diphenyltetrazolium bromide (MTT) (ACROS Organics-Antwerp, Belgium) solution was added to each well and cells were incubated for 2 h at 37 °C and 5% CO_2. After incubation supernatant was removed and 100 μL of DMSO were added to each well to dissolve formazan salts produced by active mitochondria. Absorbance (OD) was measured at λ = 570 nm in a microplate reader (Biotek Synergy-HT, Winooski, VT, USA). A minimum of three replicate wells were used for each group and at least two separate experiments were conducted. Results are expressed as mean ± SEM.

RNA extraction and quantitative real-time PCR analysis. After treatments NCTC 2544 cells were harvested and RNA extraction was performed using the Trizol reagent (Invitrogen, Carlsbad, CA, USA). First-strand cDNA was then synthesised with the Applied Biosystem (Foster City, CA, USA) reverse transcription reagent. Quantitative RT-PCR analysis was performed in Step One Fast Real-Time PCR System Applied Biosystems using the SYBR Green PCR Master Mix (Life Technologies, Monza MB, Italy) to evaluate gene expression of IL-6, IL-8 and IL-10. Results were normalized with the housekeeping gene GAPDH using a comparative $2^{-\Delta\Delta Ct}$ method.

Determination of lactic dehydrogenase release. To evaluate the presence of cell necrosis as a result of cell membrane rupture, lactic dehydrogenase (LDH) release was spectrophotometrically measured. Enzyme activity was measured at λ = 340 nm in both culture medium and cellular lysates, following β-nicotinamide-adenine dinucleotide (NADH) reduction. Results are expressed as the percentage of LDH release.

Statistical analysis

At least three independent experiments were performed for each analysis. The statistical significance (p < 0.05) of the differences between the experimental groups was determined

by Fisher's method for analyses of multiple comparisons. For comparison between treatment groups, the null hypothesis was tested *via* either a single-factor analysis of variance (ANOVA) for multiple groups or an unpaired *t*-test for two groups. Data are presented as means ± SEM.

Conclusions

The integration of nanotechnology with health, beauty, and anti-aging products is anticipated to shape the future landscape significantly.[45–48] Consequently, while the use of nanotechnology holds great promise in a wide spectrum of fields, it is imperative to address potential negative consequences associated with nanomaterials beforehand. Comprehensive toxicity studies are essential, along with thorough investigations into the impacts of various nanomaterials used in the industry on human health and the environment.[49] Studies on skin cancer have demonstrated that encapsulating therapeutics in nanoparticles enhances efficacy compared to free agents, resulting in a notable reduction in systemic and local toxicity, however obtaining good loading capacity and controlled release of most nanoparticles are the main challenges to be overcome. In this context, nanoparticles like AuNPs-SME, where the coating with snail mucus extract provides additional benefits and functions can be advantageous. In applications aimed at preventing skin cancer, our work is in line with evidence suggesting that the addition of antioxidants enhances the stability of sun-protective agents.[50] Indeed, this combined approach can be particularly significant in the context of skin cancer prevention. Despite the substantial expansion of preclinical research on nanoparticle use, its clinical application remains limited. Further studies are required to evaluate patient response to nanoparticle delivery in clinical settings. Challenges persist in manufacturing nanoparticles at a commercial scale, necessitating special attention to nanoparticle reproducibility and stability for clinical use. Nevertheless, despite these challenges, nanoparticle-based therapeutic delivery for skin cancer prevention and treatment holds significant promise in reducing skin cancer incidence and improving survivability rates, thereby benefiting populations that may have previously had limited access to optimized therapeutics.[51]

Herein, we demonstrated that snail mucus is suitable for creating innovative formulations and it can be considered valid candidate for cosmeceutical applications to enrich the snail mucus based anti-age and sunscreen products already present in the market. Innovative formulations based on nanostructured materials can be useful in improving snail mucus bioavailability. In particular SME-capped gold nanoparticles prepared by a reagent-free green one-pot synthesis represents a mild approach to integrate the properties of natural compounds with the exclusive behaviours of metal nanostructured materials.

In our experimental conditions we demonstrated that AuNPs-SME were able to modulate the inflammatory response induced by LPS in human keratinocyte cell line NCTC 2544 by significantly down-regulating the inflammatory process and selectively targeting interleukin pathway. In addition, we found that AuNPs-SME inhibited the growth of two human melanoma cell lines and did not affect immortalized human keratinocyte NCTC 2544 cells taken as non-tumorigenic cells. So AuNPs-SS can be considered an interesting cancer cells proliferation and/or metastasis inhibitor. Therefore, innovative nanotechnological formulations containing snail mucus can be used not only as anti-age and sunscreen products but also to obtain cream/gel for specific topical application in cancer treatment.

Author contributions

Conceptualization: Sorrenti V., Vanella L., Petralia S.; data curation: Montenegro L., Consoli V., Maugeri L., Satriano C.; formal analysis: Montenegro L., Consoli V., Maugeri L., Satriano C., Gulisano M.; Castellano A. Investigation: Montenegro L., Consoli V., Maugeri L., Satriano C., Gulisano M.; Petralia S.; supervision: Sorrenti V., Petralia S., Vanella L.; writing – original draft: Consoli V., Maugeri L.; writing – review & editing: Sorrenti V., Petralia S., Montenegro L.; funding acquisition: Sorrenti V.; project administration: Sorrenti V.

Conflicts of interest

There are no conflicts to declare.

Acknowledgements

This research was funded by the "SMART UP Project (PSR SICILIA 2014/20 Sottomisura 16.1—Bando 2018—D. D. S. 3092/2020 del 15/10/2020—CUP G66D20000610009)".

Notes and references

1 G. Cilia and F. Fratini, *J. Complementary Integr. Med.*, 2018, **15**(3), 20170168.
2 C. Trapella, R. Rizzo, S. Gallo, A. Alogna, D. Bortolotti, F. Casciano, G. Zauli, P. Secchiero and R. Voltan, *Sci. Rep.*, 2018, **8**, 17665.
3 D. E. López Angulo and P. J. do Amaral Sobral, *Int. J. Biol. Macromol.*, 2016, **92**, 645–653.
4 M. A. El Mubarak, F. N. Lamari and C. Kontoyannis, *J. Chromatogr. A*, 2013, **1322**, 49–53.
5 F. Pons, M. Koenig, R. Michelot, M. Mayer and N. Frossard, *Pathol. Biol.*, 1999, **47**, 73–80.
6 N. D. Rambaruth, P. Greenwell and M. V. Dwek, *Glycobiology*, 2012, **22**, 839–848.
7 M. V. Dwek, H. A. Ross, A. J. Streets, S. A. Brooks, E. Adam, A. Titcomb, J. V. Woodside, U. Schumacher and A. J. Leathem, *Int. J. Cancer*, 2001, **95**, 79–85.
8 S. A. Brooks and A. J. Leathem, *Lancet*, 1991, **338**, 71–74.
9 R. Conte, *Int. J. Nano Dimens.*, 2016, **7**(3), 181–185.
10 J. Gubitosa, V. Rizzi, P. Fini, A. Laurenzana, G. Fibbi, C. Veiga-Villauriz, F. Fanelli, F. Fracassi, A. Onzo, G. Bianco, C. Gaeta, A. Guerrieri and P. Cosma, *Soft Matter*, 2020, **16**, 10876–10888.
11 V. Rizzi, J. Gubitosa, P. Fini, S. Nuzzo, A. Agostiano and P. Cosma, *J. Photochem. Photobiol., B*, 2021, **224**, 112309.

12 M. F. Di Filippo, V. Di Matteo, L. S. Dolci, B. Albertini, B. Ballarin, M. C. Cassani, N. Passerini, G. A. Gentilomi, F. Bonvicini and S. Panzavolta, *Nanomaterials*, 2022, **12**, 3447.
13 A. A. El-Attar, H. B. El-Wakil, A. H. Hassanin, B. A. Bakr, T. M. Almutairi, M. Hagar, B. H. Elwakil and Z. A. Olama, *Membranes*, 2022, **12**, 536.
14 P. C. Mane, S. A. R. Sayyed, D. D. Kadam, M. D Shinde, A. Fatehmulla, A. M. Aldhafiri, E. A. Alghamdi, D. P. Amalnerkar and R. D. Chaudhari, *Sci. Rep.*, 2021, **11**, 13068.
15 P. Das, M. Sherazee, P. K. Marvi, S. R. Ahmed, A. Gedanken, S. Srinivasan and A. R. Rajabzadeh, *ACS Appl. Mater. Interfaces*, 2023, **15**, 29425–29439.
16 P. Das, S. Ganguly, S. R. Ahmed, M. Sherazee, S. Margel, A. Gedanken, S. Srinivasan and A. R. Rajabzadeh, *ACS Appl. Polym. Mater.*, 2022, **4**, 9323–9340.
17 M. A. Khan, M. Zafaryab, S. H. Mehdi, I. Ahmad and M. M. Rizvi, *Int. J. Biol. Macromol.*, 2016, **93**, 242–253.
18 F. Adaileh, W. Alshaer, H. Nsairat, D. A. Alqudah, S. Wehaibi, F. Daoud, R. Al-Buqain, S. Alsotari, A. Al Bawab and F. Odeh, *J. Drug Delivery Sci. Technol.*, 2023, **87**, 104886.
19 F. Rodríguez, P. Caruana, N. De la Fuente, P. Español, M. Gámez, J. Balart, E. Llurba, R. Rovira, R. Ruiz, C. Martín-Lorente, J. L. Corchero and M. V. Céspedes, *Biomolecules*, 2022, **12**, 784.
20 E. Pérez-Herrero and A. Fernández-Medarde, *Eur. J. Pharm. Biopharm.*, 2015, **93**, 52–79.
21 G. M. L. Consoli, M. L. Giuffrida, C. Satriano, T. Musumeci, G. Forte and S. Petralia, *Chem. Commun.*, 2022, **58**, 3126–3129.
22 G. M. L. Consoli, L. Maugeri, G. Forte, G. Buscarino, A. Gulino, L. Lanzanò, P. Bonacci, N. Musso and S. Petralia, *J. Mater. Chem. B*, 2024, **12**, 952–961.
23 G. M. L. Consoli, G. Forte, L. Maugeri, V. Consoli, V. Sorrenti, L. Vanella, G. Buscarino, S. Agnello, M. Camarda, G. Granata, L. Ferreri and S. Petralia, *ACS Appl. Nano Mater.*, 2023, **6**, 358–369.
24 L. Vanella, V. Consoli, I. Burò, M. Gulisano, M. S. Giglio, L. Maugeri, S. Petralia, A. Castellano and V. Sorrenti, *Int. J. Mol. Sci.*, 2023, **24**, 10185.
25 C. E. A. Botteon, L. B. Silva, G. V. Ccana-Ccapatinta, T. S. Silva, S. R. Ambrosio, R. C. S. Veneziani, J. K. Bastos and P. D. Marcato, *Sci. Rep.*, 2021, **11**, 1974.
26 E. B. Houshmand, *J. Cosmet., Dermatol.*, 2021, **20**, 776–780.
27 Z. Selamoglu, C. Dusgun, H. Akgul and M. F. Gulhan, *Iran. J. Pharm. Res.*, 2017, **16**, 92–98.
28 D. Xian, X. Gao, X. Xiong, J. Xu, L. Yang, L. Pan and J. Zhong, *J. Photochem. Photobiol., B*, 2017, **175**, 73–82.
29 V. H. P. Infante, P. M. B. G. Maia Campos, L. S. Calixto, M. E. Darvin, M. Kröger, S. Schanzer, S. B. Lohan, J. Lademann and M. C. Meinke, *Int. J. Pharm.*, 2021, **598**, 120262.
30 C. Jennifer, V. R. Gubitosa, V. Rizzi, P. Fini and Pinalysa, in *Nanocosmetics*, ed. A. Nanda, S. Nanda, T. A. Nguyen, S. Rajendran and Y. Slimani, Elsevier, 2020, pp. 349–373.
31 A. Dimitrovska Cvetkovska, S. Manfredini, P. Ziosi, S. Molesini, V. Dissette, I. Magri, C. Scapoli, A. Carrieri, E. Durini and S. Vertuani, *Int. J. Cosmet. Sci.*, 2017, **39**, 310–319.
32 M. Pissavini, C. Tricaud, G. Wiener, A. Lauer, M. Contier, L. Kolbe, C. Trullás Cabanas, F. Boyer, E. Meredith, J. de Lapuente, E. Dietrich and P. J. Matts, *Int. J. Cosmet. Sci.*, 2020, **42**, 421–428.
33 E. P. Santos, Z. M. Freitas, K. R. Souza, S. Garcia and A. Vergnanini, *Int. J. Cosmet. Sci.*, 1999, **21**, 1–5.
34 C. D. Kaur and S. Saraf, *Pharmacogn. Res.*, 2010, **2**, 22–25.
35 G. Netto MPharm and J. Jose, *J. Cosmet., Dermatol.*, 2018, **17**, 1073–1083.
36 J. Jose and G. Netto, *J. Cosmet., Dermatol.*, 2019, **18**, 315–321.
37 S. A. Wissing and R. H. Müller, *Pharmazie*, 2001, **56**, 783–786.
38 M. Goldfeder, M. Kanteev, S. Isaschar-Ovdat, N. Adir and A. Fishman, *Nat. Commun.*, 2014, **5**, 4505.
39 Y. Pu, B. Zhou, H. Xiang, W. Wu, H. Yin, W. Yue, Y. Yin, H. Li, Y. Chen and H. Xu, *Biomaterials*, 2020, **259**, 120329.
40 C. Ellijimi, M. Ben Hammouda, H. Othman, W. Moslah, J. Jebali, H. B. Mabrouk, M. Morjen, M. Haoues, J. Luis, N. Marrakchi, K. Essafi-Benkhadir and N. Srairi-Abid, *Biomed. Pharmacother.*, 2018, **101**, 871–880.
41 N. Noothuan, K. Apitanyasai, S. Panha and A. Tassanakajon, *BMC Res. Notes*, 2021, **14**, 138.
42 D. K. Roper, W. Ahn and M. Hoepfner, *J. Phys. Chem. C*, 2007, **111**, 3636–3641.
43 E. Abreu Dutra, D. A. Gonçalves da Costa e Oliveira, E. R. M. Kedor-Hackmann and M. I. R. Miritello Santoro, *Rev. Bras. Cienc. Farm.*, 2004, **40**(3), DOI: **10.1590/S1516-93322004000300014**.
44 R. M. Sayre, P. P. Agin, G. J. LeVee and E. Marlowe, *Photochem. Photobiol.*, 1979, **29**, 559–566.
45 K. Mitri, R. Shegokar, S. Gohla, C. Anselmi and R. H. Müller, *Int. J. Pharm.*, 2011, **420**, 141–146.
46 E. Zingale, A. Bonaccorso, C. Carbone, T. Musumeci and R. Pignatello, *Pharmaceutics*, 2022, **14**, 691.
47 S. Kaul, N. Gulati, D. Verma, S. Mukherjee and U. Nagaich, *J. Pharm.*, 2018, **2018**, 3420204.
48 S. Shanbhag, A. Nayak, R. Narayan and U. Y. Nayak, *Adv. Pharm. Bull.*, 2019, **9**, 348–359.
49 C. Cardoza, V. Nagtode, A. Pratap and S. N. Mali, *Health Sci. Rev.*, 2022, **4**, 100051.
50 J. F. Nash, *Dermatol. Clin.*, 2006, **24**, 35–51.
51 J. Chang, B. Yu, W. M. Saltzman and M. Girardi, *JID Innov.*, 2023, **3**, 100197.